Galiana-Merino, J. J., Parolai, S., Rosa-Herranz, J. (2011): Seismic wave characterization using complex trace analysis in the stationary wavelet packet domain. - Soil Dynamics and Earthquake Engineering, 31, 11, 1565-1578

DOI: 10.1016/j.soildyn.2011.06.009

Seismic Wave Characterization Using Complex Trace Analysis In the Stationary Wavelet Packet Domain

J.J. Galiana-Merino[1,2], S. Parolai[3] and J. Rosa-Herranz[1,2]

[1]Dept. Physics, Systems Engineering and Signal Theory, University of Alicante, P.O.Box 99, E-03080 Alicante, Spain

[2]University Institute of Physics Applied to Sciences and Technologies University of Alicante, Spain

[3] GFZ German Research Center for Geosciences, Telegrafenberg, 14473 Potsdam, Germany

E-mail: juanjo@dfists.ua.es, parolai@gfz-potsdam.de, julio@dfists.ua.es

Abstract

One of the most important tasks in seismology and applied geophysics is the identification of the different kinds of waves that form a seismic record by means of polarization analysis. In particular, this involves the extraction of body waves (linear polarization) or surface waves (mostly elliptical polarization) from a set of seismic data and which forms a key point in several studies.

In this work, a new method of time-frequency polarization analysis based on the stationary wavelet packet transform is developed. The proposed approach identifies and extracts automatically the different waves included in the signal, dependent upon the reciprocal ellipticity. Moreover, the algorithm provides enough information to the user to allow them to also manually select the reciprocal ellipticity intervals, and then extract the corresponding waves of interest contained in the signals.

The proposed polarization estimation method and the automatic features extraction algorithm have been evaluated first using synthetic signals, and then applied to real seismic records. Based on the results obtained from both synthetic and real signals, we can conclude that the proposed method correctly identifies and extracts automatically the linearly and ellipticaly polarized waves from the signal, discerning clearly both types of polarization. Moreover, the proposed method is able to identify and extract signals with different kinds of elliptical polarization, allowing us to understand better the characteristics of Rayleigh waves.

Index Terms – Polarization analysis, wave identification, seismic signal processing, stationary wavelet packet transform (SWPT).

Introduction

One of the most important tasks in seismology and applied geophysics is the identification and extraction of the different types of waves that form a seismic record by means of polarization analysis. This involves the extraction of body waves (linear polarization) or surface waves (mostly elliptical polarization) from a set of seismic data.

Rayleigh waves are dispersive when they propagate along a vertically heterogeneous medium. Due to the subsoil structure, their velocity and polarization properties have a high dependence on the frequency and mode of propagation (Shieh and Herrmann, 1990). The estimation of the frequency-dependent velocities (dispersion curves) is therefore a crucial point when conducting site effect assessments by ambient vibrations (Scherbaum et al., 2003; Ohrnberger et al., 2003; Parolai et al., 2006; Richwalski et al., 2007).

Vidale (1986), René et al. (1986) and Li and Crampin (1991) proposed different time-domain methods based on complex trace analysis (CTA) and defined the instantaneous polarization attributes for the Rayleigh and shear-wave identification. These methods analyze only the vertical and radial components. Morozov and Smithson (1996) proposed a variational method, which allows the generalization to any number of components and therefore the identification of Love waves.

The CTA method analyzes seismic data as analytic signals, which enables the local characteristics of the signal to be maintained, providing the instantaneous

amplitude and phase. The concept of the complex analytic signal was first introduced by Gabor (1946) for the study of the minimum bandwidth needed for the transmission of radio and television signals. In seismology, Farnbach (1975) applied CTA analysis to estimating the enveloped and the instantaneous phase of the seismic records and subsequently the arrival time of the different seismic waves. Taner and Sheriff (1977) and Taner et al. (1979) also applied CTA analysis to single-component seismic data and defined the concepts of reflection strength and reflection polarity as the instantaneous amplitude and the sign of the instantaneous phase, respectively. René et al. (1986) defined the complex multicomponent signal, with the real orthogonal components, that correspond to the registered components, and the imaginary components, obtained by applying the Hilbert transform to the real components. They characterized the polarization of the seismic waves through instantaneous and mean polarization attributes, such as the phase difference, the reciprocal ellipticity and the tilt angle.

In all of the above mentioned studies, the CTA analysis is applied in the time domain and therefore, no frequency information is provided. In this way, the instantaneous polarization attributes represent mean values for the complete frequency range of the signal.

When the different types of waves contained in one signal do not interfere over the same interval times, the CTA analysis provides good results and is able to identify the different waves. However, this is not the case for the most of the observed seismograms, where the Rayleigh waves (elliptically polarized) appear together with some others, for example, reflection modes of the body waves (linearly

polarized). This is the reason why a time-frequency polarization analysis seems to be a more appropriate alternative in order to separate the different phases in the wavefield. A similar aim guided the studies of Diallo et al. (2005, 2006) and Kulesh et al. (2007, 2008), where the time-frequency polarization analysis is carried out using the Continuous Wavelet Transform (CWT).

Considering that geophysicists are always nowadays working with discrete time signals, the use of a continuous transform such as the CWT might not always be the most appropriate tool for such analysis. The CWT application requires a transform discretization, where the discrete signal is analyzed in a finite set of scales and for some finite numbers of translations. This is not a serious drawback if the only purpose of the time-frequency analysis involves estimating some characteristics of the signal, for example the P-wave onset. However, for some applications, such as those of interest in this study where the aim is to identify and separate the different kind of waves contained in the seismic signal, the use of the inverse transform for recovering the waves in the time domain might be limited. In fact, although the definition of the inverse transform is well established, with its expression and its applicability conditions, it is not possible to recover the original signal when only a discrete set of scales and translation values has been applied for obtaining the CWT coefficients. In this situation, some approximated inversion methods can be applied for returning to the time-domain, as explained in Diallo et al. (2006).

Considering the discrete data used in geophysics and the necessity of performing the final analysis in the time domain, it seems more appropriate to use other kind of time-frequency transforms, i.e., discrete transforms such as the Discrete

Wavelet Transform (DWT) or the Discrete Wavelet Packet Transform (DWPT). Previous studies have used the DWT to perform polarization analysis with different aims (e.g., Anant and Dowla, 1997; Galiana-Merino et al., 2007; D'Auria et al., 2010). However, among these discrete transforms, the DWPT provides the greater flexibility for the analysis of the different frequency bands in which the signal can be decomposed. DWPT allows us to analyze the signal at different frequency bands, without being forced to assign more relevance to any of them, as required when using DWT.

The above mentioned wavelet based transforms (CWT, DWT or DWPT) are time-shift transforms. This implies that the corresponding wavelet coefficients could suffer from some distortion or time shift, depending on the initial sample. In the present study, we aim at estimating the instantaneous polarization parameters in the time-frequency domain, and thus any phase variation of the wavelet coefficients would lead to erroneous results. Diallo et al. (2006) used a complex wavelet as the mother wavelet, which has the advantage, compared with the real ones, that it does not introduce any phase distortion. Specifically, they used the complex Morlet wavelet.

In order to avoid this restriction, in this work we have developed a new method for the polarization analysis in the time-frequency domain based on the Discrete Stationary Wavelet Packet Transform (DSWPT). DSWPT does not introduce any phase distortion, independent of the mother wavelet, complex or real, used. In this way, we can apply other kinds of real wavelets, with shapes similar to the studied seismic waves. This approach , which has several advantages with respect

to the CWT based methods and obviously, with respect to methods based on time domain analysis only. In particular, in contrast to methods based on CWT, the proposed method provides a perfect reconstruction from the time-frequency domain to the time domain. This allows us to decompose the original signal in different waves, depending on their polarization, without any loss of information. Moreover, it provides flexibility in the mother wavelet selection, as it does not require any restriction on using any real or complex wavelet.

In addition to the development and implementation of the proposed method, we have also developed an algorithm for the automatic identification and extraction of the different waves included in the signal, depending on the reciprocal ellipticity. The proposed algorithm also provides enough information to the users so that they can extract manually the waves associated with any range of reciprocal ellipticity.

The proposed method and the automatic extraction of the waves have been first tested on synthetic signals. Due to the excellent results obtained for all the analyzed synthetic cases, they have been applied to real seismic data. The results are discussed in terms of the linearly and elliptically polarized waves automatically estimated from the analyzed signals.

2. Mathematical background

2.1. The Wavelet Packet and Stationary Wavelet Packet Transform

For the case of non-stationary signals, a time-frequency analysis is more appropriate than separate analyses in the time or frequency domains alone (Steeghs, 1997). Some examples of time-frequency analysis are the DWT (Daubechies, 1992; Wickerhauser,

1994) and the DWPT (Wickerhauser, 1994).

The DWT analysis supposes intrinsically that the spectral information is contained at lower frequencies, where the time-frequency decomposition follows a fixed scheme with a logarithmic tree structure. This is not necessarily appropriate for all the signals, as it is the case of the seismic data. The DWPT generalizes the wavelet analysis and allows the decomposition of the time-frequency plane in such a way that it conveniently suits the signals under study.

The DWPT is implemented using a sub-band coding scheme based on H and G filters that represent low-pass and high-pass filters, respectively, and on a downsampling operator D, that simply chooses every even sample of a sequence (Figure 1).

The original signal $s(n)$ is represented by $\lambda_{0,0}(n)$. At each scale, *j*, of the DWPT, there are 2^j independent signals (nodes or wavelet packet coefficients) and every one of them provides two outputs:

$$\begin{aligned} \lambda_{j+1,2r}(n) &= DH\,\lambda_{j,r}(n) \\ \lambda_{j+1,2r+1}(n) &= DG\,\lambda_{j,r}(n) \\ j &= 0,....,L-1 \end{aligned} \tag{1}$$

where *n* is the sample index, *j* is the scale parameter, *L* is the maximum decomposition level and *r* represents the frequency index for a given scale and varies from 0 to 2^j-1. In this way, at a given scale *L*, we obtain a set of signals $\left\{\lambda_{L,0}(n),\lambda_{L,1}(n),...,\lambda_{L,2^L-1}(n)\right\}$ which is an alternative representation of $\lambda_{0,0}(n)$ and

from which the original signal can be reconstructed perfectly (Wickerhauser, 1994). More details about the DWPT can also be found in Galiana-Merino et al. (2003).

The DWT and DWPT are shift-variant transforms due to the downsampling operation. This means that the DWT (or DWPT) of a translated version of a signal $s(n)$ is not, in general, the translated version of the DWT (or DWPT) of $s(n)$. For some applications, like filtering processes, this may not be an important issue as the signal is exactly recovered after applying the inverse transform. For other applications, however, such as the present one, where the polarization study is carried out in the wavelet packet domain, shift-variant is a serious drawback.

To overcome this problem, the basic DWPT algorithm can be modified to provide a version of DSWPT that no longer depends on translations of the signal. The modification is similar to the Discrete Stationary Wavelet Transform (Nason and Silverman, 1995; Galiana-Merino et al., 2008).

The DSWPT is implemented using the same sub-band coding scheme. In this case, the appropriate low and high pass filters are applied to the data at each scale, but no downsampling is performed. Instead, the filters are modified at each scale by applying an operator *I*, which inserts a zero between every adjacent pair of elements, as follows:

$$H_{j+1} = I H_j \quad \Rightarrow \begin{cases} h_{j+1}(2k) & = h_j(k) \\ h_{j+1}(2k+1) & = 0 \end{cases} \tag{2}$$

$$j = 0,....,L-2$$

where *k* is the sample index of the filter.

The stationary wavelet packet coefficients can be calculated recursively in the

following way:

$$\lambda^{sta}_{j+1,2r}(n) = H_j\, \lambda^{sta}_{j,2r}(n)$$

$$\lambda^{sta}_{j+1,2r+1}(n) = G_j\, \lambda^{sta}_{j,2r+1}(n) \tag{3}$$

$$j = 0,....,L-1$$

where n is the sample index, j is the scale parameter, L is the maximum decomposition level and r is the frequency index for a given scale.

Supposing that the wavelet packet basis (set of different nodes or signals covering the full frequency band) is composed of the stationary wavelet packet coefficients associated with the maximum scale, L, as is the case of the proposed method, the original signal, $\lambda_{0,0}(n)$ can be represented as $\left\{\lambda^{sta}_{L.0}(n), \lambda^{sta}_{L,1}(n), \lambda^{sta}_{L,2}(n), ..., \lambda^{sta}_{L,2^L-1}(n)\right\}$, where all coefficients have the same length as the original signal, rather than becoming shorter as the scale increases, as is the case in standard DWPT.

Moreover, the original signal can be exactly recovered by only adding all the stationary wavelet packet coefficients of the maximum scale.

$$\lambda_{0,0}(n) = \lambda^{sta}_{L.0}(n) + \lambda^{sta}_{L,1}(n) + \lambda^{sta}_{L,2}(n) + ... + \lambda^{sta}_{L,2^L-1}(n) \tag{4}$$

2.2. Polarization analysis in the time-frequency domain

In this section, the methodology used for estimating the instantaneous polarization parameters in the time-frequency domain is explained in detail.

Let $\mathrm{s}(n)$ be a three-component seismic signal, which can be represented as

$$\boldsymbol{s}(n) = \{s_i(n)\} \qquad i = x,y,z \tag{5}$$

For each component, the associated analytic complex signals can be obtained by

$$c_i(n) = s_i(n) + i \cdot H\{s_i(n)\} \tag{6}$$

where $H\{s_i(n)\}$ is the Hilbert transform of the real signal $s_i(n)$.

The analytic complex signal can be calculated through the following steps: 1) completing with zeros the signal until the number of samples is equal to a power of two equals or higher than twice the length of the original signal, 2) applying the Fast Fourier Transform (FFT), 3) the values corresponding to the negative frequencies are set to zero and the values corresponding to the positive frequencies are doubled, 4) finally, the inverse FFT is applied.

The application of the DSWPT on the $c_i(n)$ signals results in a set of coefficients, $\lambda_{j,r}^{sta}(n)\big|_{c_i}$, that are associated with the different nodes of the wavelet packet basis.

In our case, the selected wavelet packet basis is composed of the coefficients associated with the maximum scale $\left\{\lambda_{L,0}^{sta}(n)\big|_{c_i}, \lambda_{L,1}^{sta}(n)\big|_{c_i}, \lambda_{L,2}^{sta}(n)\big|_{c_i}, ..., \lambda_{L,2^L-1}^{sta}(n)\big|_{c_i}\right\}$

Due to the linear property of the DSWPT, the coefficients $\lambda_{L,r}^{sta}(n)\big|_{c_i}$ can be divided in two groups, corresponding to the real and imaginary parts of the analytic complex signal. In this way, the coefficients obtained from the DSWPT can be expressed as

$$\lambda_{L,r}^{sta}(n)\big|_{c_i} = \lambda_{L,r}^{sta}(n)\big|_{s_i} + \lambda_{L,r}^{sta}(n)\big|_{H\{s_i\}} \tag{7}$$

where $\lambda_{L,r}^{sta}(n)\big|_{c_i}$ is the set of coefficients associated with the analytic complex signal, $\lambda_{L,r}^{sta}(n)\big|_{s_i}$ is the set of coefficients associated with the recorded signal (real part of $c_i(n)$), and $\lambda_{L,r}^{sta}(n)\big|_{H\{s_i\}}$ is the set of coefficients associated with the Hilbert transform of the recorded signal (imaginary part of $c_i(n)$).

The analysis of these sets of coefficients as analytic complex signals allows us to maintain the local properties of the signal and then, estimate the instantaneous amplitude and phase for all the points (n, r) in the time-frequency domain.

$$A_i(n,r) = \sqrt{\left(\lambda_{L,r}^{sta}(n)\big|_{s_i}\right)^2 + \left(\lambda_{L,r}^{sta}(n)\big|_{H\{s_i\}}\right)^2} \tag{8}$$

$$\theta_i(n,r) = \arctan\left(\frac{\lambda_{L,r}^{sta}(n)\big|_{H\{s_i\}}}{\lambda_{L,r}^{sta}(n)\big|_{s_i}}\right) \tag{9}$$

For the subsequent polarization analysis, any combination of two orthogonal components could be selected. However, for the characterization of the Rayleigh waves, the most appropriate is to select the set of coefficients associated with the vertical component, $\lambda_{L,r}^{sta}(n)\big|_{c_z}$ and the set of coefficients associated with the horizontal component aligned with the incoming direction of the seismic wave, ($\lambda_{L,r}^{sta}(n)\big|_{c_x}$ or $\lambda_{L,r}^{sta}(n)\big|_{c_y}$). From now on, we denote both horizontal components using the subscript h (e.g., $\lambda_{L,r}^{sta}(n)\big|_{c_h}$).

The time-frequency polarization attributes of the seismic signal can now be obtained by an extension of the analysis shown by Taner et al. (1979) for the time domain. In this way, the four geometric parameters that characterize the attributes of the elliptical polarization can be defined in the time-frequency domain as (Figure 2):

1) $a(n,r) \rightarrow$ semi-major axis

2) $b(n,r) \rightarrow$ semi-minor axis

3) $\phi(n,r) \rightarrow$ phase difference between the vertical component, $\lambda_{L,r}^{sta}(n)\big|_{c_z}$, and the horizontal component, $\lambda_{L,r}^{sta}(n)\big|_{c_h}$.

4) $\tau(n,r) \rightarrow$ tilt angle of the polarization ellipse with respect to the vertical

Therefore, the instantaneous phase difference between the set of coefficients of both components is expressed as:

$$\phi(n,r) = \arctan\left(\frac{\lambda_{L,r}^{sta}(n)\big|_{s_h} \cdot \lambda_{L,r}^{sta}(n)\big|_{H\{s_z\}} - \lambda_{L,r}^{sta}(n)\big|_{s_z} \cdot \lambda_{L,r}^{sta}(n)\big|_{H\{s_h\}}}{\lambda_{L,r}^{sta}(n)\big|_{s_z} \cdot \lambda_{L,r}^{sta}(n)\big|_{s_h} + \lambda_{L,r}^{sta}(n)\big|_{H\{s_z\}} \cdot \lambda_{L,r}^{sta}(n)\big|_{H\{s_h\}}} \right) \tag{10}$$

With respect to the instantaneous values of the semi-major and semi-minor axes, these can be estimated by the following equations

$$a(n,r) = \left(\frac{S_0(n,r) + \left(S_1^2(n,r) + S_2^2(n,r) \right)^{1/2}}{2} \right)^{1/2} \tag{11}$$

$$b(n,r) = \left(\frac{S_0(n,r) - \left(S_1^2(n,r) + S_2^2(n,r) \right)^{1/2}}{2} \right)^{1/2} \tag{12}$$

where S_0, S_1 y S_2 are the three Stoke parameters (René et al., 1986), which can be obtained by:

$$S_0(n,r) = A_z^2(n,r) + A_h^2(n,r) \tag{13}$$

$$S_1(n,r) = A_z^2(n,r) - A_h^2(n,r) \tag{14}$$

$$S_2(n,r) = 2 \cdot A_z(n,r) \cdot A_h(n,r) \cdot \cos\left(\phi(n,r)\right) \tag{15}$$

Finally, the tilt angle, τ, can be also calculated by using the Stoke parameters, as:

$$\tau(n,r) = \frac{1}{2} \cdot \arctan\left(\frac{S_2(n,r)}{S_1(n,r)}\right) \tag{16}$$

From the obtained semi-major and semi-minor axes values, the instantaneous reciprocal ellipticity and the signed instantaneous reciprocal ellipticity are defined, respectively, as:

$$\varphi(n,r) = \frac{b(n,r)}{a(n,r)} \tag{17}$$

$$\sigma(n,r) = sign\left(\phi(n,r)\right) \cdot \varphi(n,r) \tag{18}$$

Theoretically, for linear polarization, the reciprocal ellipticity is zero, i.e., $\varphi(n,r) = 0$, while for circular polarization $\varphi(n,r) = 1$. Considering $\sigma(n,r)$, it is positive or negative, depending on the movement counter-clockwise or clockwise of the ellipse, respectively.

As we work with instantaneous values, artifacts or instabilities could appear at some points of the reciprocal ellipticity plane. In the time domain, René et al. (1986) averaged the instantaneous parameters in order to smooth the results and avoid possible artifacts. Following a similar scheme, in this work we propose to apply a 2D median filter to reduce the instantaneous instabilities or artifacts in the reciprocal ellipticity plane.

2.3. Design of polarization filters

Once we have the different polarization attributes in the time-frequency domain, it is possible to design filters that allow different phases to be identified based on selected attributes of the parameters considered. The reciprocal ellipticity is one of the most significant when discerning the different waves contained in a seismic signal. Depending on its value, the wave polarization can be classified as linear, elliptical or circular. The DSWPT coefficients can therefore be selected and the desired polarization characteristics extracted.

In this work, we use a filter based on the 'hard thresholding' method (Donoho and Johnstone, 1994) where the threshold is estimated as a function of the reciprocal ellipticity instead of as a function of the noise level. The most important difference when compared to the common application of the 'hard thresholding' method is that the selection criterion is based on the distribution in the time-frequency plane of the reciprocal ellipticity. Furthermore, the modified coefficients correspond to the time-frequency plane representation of the analytic complex signal. Mathematically, the proposed filtering can be expressed as:

$$\hat{\lambda}^{sta}_{L,r}[n]\Big|_{c_i} = \begin{cases} 0 & if \;\; \varphi(n,r) < \varphi_{\min} \;\; or \;\; \varphi(n,r) > \varphi_{\max} \\ \lambda^{sta}_{L,r}(n)\Big|_{c_i} & if \;\; \varphi_{\min} \le \varphi(n,r) \le \varphi_{\max} \end{cases} \quad (19)$$

Following this criterion, the coefficients corresponding to the vertical and horizontal components of the signal, $\hat{\lambda}^{sta}_{L,r}(n)\Big|_{c_i}$, should be modified.

3. Proposed method

3.1. Polarization attributes in the time-frequency domain

In this section, we explain the implementation of the proposed polarization analysis, involving an algorithm developed for the extraction, automatic and manual, of the different waves contained in the signal, according to the reciprocal ellipticity. Figure 3 shows the general scheme of the proposed method.

The first six steps are basically the implementation of the equations presented in section 2.2. For the DSWPT analysis, we used the Daubechies 12 as the mother wavelet, which is appropriate for the analysis of seismic signals (Galiana-Merino et al., 2003). The maximum level of decomposition is fixed to 8. Since no selection has been done with respect to the best basis of the wavelet packet transform, the number of nodes corresponds to the number of nodes of the maximum level (2^8=256). In this way, the frequency band of the signal is divided in 256 bands of the same width.

The recorded signal is a matrix of size n x 3, which contains n samples in the time domain for the three components: vertical, radial and transversal. After the DSWPT, the signal is transformed in a matrix of size n x 256 x 3, where each component is represented by n x 256 points in the time-frequency plane. In Figure 4,

an example of the vertical component of a real signal and its corresponding DSWPT coefficients is shown.

Once the signal is converted to the time-frequency domain, the polarization attributes are calculated at every point of this plane, following the equations of section 2.2. Then the instantaneous amplitude and phase, the geometric parameters of the polarization ellipse and the instantaneous reciprocal ellipticity are then calculated (e.g. Figure 4c).

Finally, a 2D median filter is applied to the reciprocal ellipticity matrix to smooth the obtained values and reduce possible instantaneous instabilities and artifacts. In the present work, the time-frequency dimension of the applied median filter has been set at 50 samples x 3 frequency bands, as a compromise between smoothing and artifacts, but this is user configurable.

3.2. Automatic extraction of seismic waves

The last two steps of the procedure, 7 and 8, focus on the analysis of the reciprocal ellipticity that characterizes the signal, and the subsequent extraction of the different waves contained in the signal.

In step 7, a filter bank of reciprocal ellipticity has been applied to the set of coefficients, $\lambda_{L,r}^{sta}(n)\big|_{c_i}$. The bandwidth of the filters, following equation 19, is determined by the $\varphi_{\min}$ and $\varphi_{\max}$ values. In such a filter, $\varphi_{\min}$ is set to 0, while $\varphi_{\max}$ is increased progressively in steps of $\Delta\varphi$ until the maximum value of reciprocal

ellipticity is reached, i.e., 1. In Figure 5, the scheme of the filter bank of reciprocal ellipticity is shown.

$\Delta\varphi$ is a parameter that can be adjusted by the user in order to modify the resolution of the analysis. For the synthetic and real signals analyzed in this work, we have chosen $\Delta\varphi = 0.025$, which in our experience has provided very good results in the separation of the synthetic waves (see section 4).

After filtering, the inverse transform is used for retrieving the sub-signals corresponding to each reciprocal ellipticity band in the time domain. The differences between sub-signals corresponding to contiguous reciprocal ellipticity bands are also plotted in order to better identify the changes.

The automatic selection of the waves contained in the original signal is carried out based on the correlation analysis of the sub-signals representing consecutive reciprocal ellipticity bands. If these consecutive sub-signals do not present significant differences, the correlation will be close to 1. In contrast, if some change occurs between consecutive sub-signals, the correlation will be less than 1, indicating the presence of some new wave of the signal, with different reciprocal ellipticity.

Based on this criterion, the algorithm automatically detects the local minima of the correlation results and then selects the reciprocal ellipticity ranges comprised between two local minima. These reciprocal ellipticity ranges correspond to the different waves contained in the original signal. The results obtained by the correlation analysis are shown graphically and in a table in order to assist with the manual inspection.

4. Results and discussion

4.1. Evaluation of synthetic signals

The proposed method was tested first using synthetic signals composed of waves with different reciprocal ellipticity. One representative example of this analysis and the results obtained is shown and commented in detail in this section.

In this example, we use a synthetic signal composed of three waves with different reciprocal ellipticity. One of them is linearly polarized, meanwhile the other two have elliptical polarization. The sub-signals used are sinusoids smoothed with a hanning window. For the linearly polarized wave, the wave has a frequency of 5Hz and the linear polarization is obtained by not introducing any delay between the vertical and radial components. For the first elliptical wave, the frequency is fixed to 1Hz and the delay between the vertical and the radial components is 0.9 rad. This delay ensures that the wave is elliptically polarized, with reciprocal ellipticity equals to $\varphi(n,r) = 0.484$. Finally, the second elliptical wave is characterized by a frequency of 2Hz and a delay of 1.0 rad., which implies $\varphi(n,r) = 0.543$. The sampling rate used for generating the different waves is 100 samples per second.

In Figure 6, the vertical and radial components of the three waves, as well as the vertical and radial components of the composed synthetic signal are shown.

In Figure 7, the signal decomposition at different reciprocal ellipticity intervals (see Figure 5) and the respective differences between these intervals are shown. For the clarity of this figure, we only show the results at $\Delta\varphi = 0.1$, although the analysis was carried out using $\Delta\varphi = 0.025$, as it was pointed out in section 3.2.

The experimental tests we carried out varying the $\Delta\varphi$ value demonstrated that this step is small enough to assure a good discrimination among the different waves contained in the signal.

Next, the correlation coefficients between the different consecutive sub-signals obtained from the filtering process are calculated. The graphic results are plotted ($\Delta\varphi = 0.025$) in Figure 8 and the results at intervals of $\Delta\varphi = 0.1$ are shown in Table 1.

The reciprocal ellipticity of the linearly polarized wave is close to 0. We can see that the correlation coefficient (Figure 8) is constant and close to 1 for values of the reciprocal ellipticity between 0 and 0.475. At 0.475, a local minimum of the correlation coefficient is observed, which may be indicative of the presence of a new wave in the signal that is different to the previous one. In the analyzed case, this change is due to the presence of the first elliptically polarized wave, $\varphi(n,r) = 0.484$. After reaching a minimum value, the correlation coefficient increases again to 1 (at 0.500). If it was the only elliptically polarized wave, the correlation coefficient would reach 1 and would remain constant for higher values of the reciprocal ellipticity. However, we can observe a new decrease in the correlation coefficient with the reciprocal ellipticity assuming a value of 0.525. This indicates that a new elliptically polarized wave was found in the signal, corresponding to the second elliptically polarized wave with $\varphi(n,r) = 0.543$. After reaching a minimum value, the correlation coefficient increases again to 1 and remains constant until the end of the process, indicating that no other waves are observed.

Therefore, the automatic analysis of the correlation coefficients identifies the following three different reciprocal ellipticity intervals: 0-0.475; 0.475-0.525 and 0.525-1. After filtering the time-frequency signal according to these reciprocal ellipticity ranges (see section 3.2), the three waves of the synthetic signal are retrieved accurately (Figure 9).

It is important to note that this wave identification process is carried out in an automatic mode, without any intervention from the user. However, the developed tool provides all the intermediate results (Figures 7 and 8; and Table 1), which allows the user a visual (and sometimes more accurate) inspection of the obtained results and a manual selection of the reciprocal ellipticity intervals.

In the case at hand, it is possible to compare the obtained waves with the synthetic ones, in order to evaluate the accuracy of the wave identification and separation process. In Figure 9, we can see that the graphical comparison between the estimated and synthetic waves appears very satisfactory. Moreover, in Table 2, the correlation coefficients between the estimated and the synthetic waves are also shown, with all of the waves included in the signal being accurately retrieved, with a correlation coefficient of around 0.99.

We now repeat the same example, but after adding white noise to the synthetic signal. In this case, the automatic analysis of the correlation coefficients identifies the following four different ranges of reciprocal ellipticity: 0-0.100; 0.100-0.475; 0.475-0.525 and 0.525-1 (see Figure 10). The local minimum obtained at $\varphi = 0.100$ corresponds to the presence of the first wave of the signal contaminated with noise. Below this value, there is only a small part of the linearly polarized wave

and/or only noise and spurious signals. Theoretically, the linearly polarized wave should have a reciprocal ellipticity equal to 0.000. However, in the case of signals contaminated with noise, such as the present example, the reciprocal ellipticity associated with the linearly polarized waves covers a small range of values slightly higher than zero and then, a first local minimum, which has not to be considered, use to appear. Taking this into account, the reciprocal ellipticity intervals are reduced to 0-0.475, 0.475-0.525, and 0.525-1, which are the same intervals obtained for the signal without noise.

In Figure 11, we can see the graphical comparison between the estimated and the pure synthetic waves, where the estimated waves are also contaminated with some of the noise. In Table 3, the correlation coefficients between the estimated and the synthetic waves are also shown. In this case, all the waves included in the signal have been also retrieved accurately, with a correlation coefficient around 0.99.

4.3. Application to real seismograms

The proposed method has also been applied on real seismograms recorded by a linear array of geophones, which were deployed in the city of Bonn (Germany) in October 2003 (Richwalski et al., 2007). An active experiment was carried out with a controlled source. The survey was conducted by deploying sixteen 4.5 Hz three-component geophones in a linear array of 96 m with non-regular inter spacing (Figure 12). The source was offset at 15 m from the first geophone. A sledgehammer of 40 kg was dropped from a height of 3.5 m, hitting a thick metal plate placed at one

end of the geophone line. The sampling frequency was fixed to 1000 s.p.s, with a total recording time of 2 s for each record.

The method proposed in this study has been applied to this data set, where the signals contained surface waves (elliptical polarization) as well as body waves (linear polarization) recorded by the sixteen geophones. As an example, we show the results obtained for the signal recorded by geophone 9 (Figure 13), located at 48.5 m, which is approximately in the middle of the array.

As mentioned in section 2, only the vertical and the radial components are needed for the subsequent polarization analysis since we focus on P and Rayleigh waves. The reciprocal ellipticity has been analyzed in the time-frequency plane using a step of $\Delta\varphi = 0.025$. A lower value of $\Delta\varphi$ may falsely estimate waves due to small instabilities or fluctuations between the consecutive values of the reciprocal ellipticity. In the case of choosing higher values, e.g., $\Delta\varphi = 0.100$, the process would be more robust to these fluctuations, in exchange of a low reciprocal ellipticity resolution.

In Figure 14, the correlation coefficients between the different consecutive sub-signals obtained from the filtering process are shown. From the correlation coefficient information, and after detecting the local minima on the curve, the proposed method automatically provides the reciprocal ellipticity limits associated with the different possible waves contained the signal.

In this case, these limits are the following: $\Delta\varphi_1$ = [0.000 – 0.050]; $\Delta\varphi_2$ = [0.050 – 0.175]; $\Delta\varphi_3$ = [0.175 – 0.350]; $\Delta\varphi_4$ = [0.350 – 0.400]; $\Delta\varphi_5$ = [0.400 – 0.475]; $\Delta\varphi_6$ = [0.475 – 0.525]; and $\Delta\varphi_7$ = [0.525 – 1.000].

Considering the first two intervals, $\Delta\varphi_1$ and $\Delta\varphi_2$, they should form only one, $\Delta\varphi_{1-2}$=[0.000 – 0.175]. The minimum obtained at $\varphi = 0.050$ corresponds to the presence of the first wave of the signal. In fact, below this value, there is no significant wave in the signal. Theoretically, the body waves (linearly polarized) should have a reciprocal ellipticity equal to 0.000. However, in the case of real seismograms, the signal is contaminated with noise and therefore the reciprocal ellipticity associated with body waves will not be exactly equal to zero. In fact, the reciprocal ellipticity will be slight higher than zero and its value will depend on the signal to noise ratio of the recorded seismograms. In conclusion, with this modifications, the first two intervals are $\Delta\varphi_{1-2}$=[0.000 – 0.175] and $\Delta\varphi_3$ = [0.175 – 0.350].

After checking the results provided by the automatic process (not shown here for simplicity), it seems that the waves obtained for the intervals $\Delta\varphi_6$ and $\Delta\varphi_7$ may also be joined in one interval $\Delta\varphi_{6-7}$=[0.4750 – 1.000]. As the reciprocal ellipticity increment is small, in some cases, the obtained correlation coefficient curve may present some slight local minima, which split a reciprocal ellipticity interval into two and therefore extract two waves from the signal where there should be only one. This is the situation that occurs at 0.525, where there is a very slight decrease in the correlation coefficient and then the automatic process selects two reciprocal ellipticity intervals at $\Delta\varphi_6$ = [0.450 – 0.525]; and $\Delta\varphi_7$ = [0.525 – 1.000].

In Figure 15, the estimated waves are shown. The first interval, $\Delta\varphi_{1-2}$=[0.000 – 0.175], may correspond to body waves (linearly polarized), meanwhile the rest of

the estimated waves may be associated with surface waves with different elliptical polarizations. In this case, although the body waves present a very low amplitude with respect to the amplitudes of the Rayleigh waves, they can still be identified and extracted from the original seismogram.

As we can see, the automatic process provides an initial and rough selection of the different kinds of waves contained in the signal, based on the reciprocal ellipticity of these waves. The procedure can, of course, be refined by adjusting the reciprocal ellipticity intervals, if necessary.

5. Conclusions

In this work, a new method for polarization analysis in the time-frequency domain based on SDWPT has been developed.

The proposed method presents some advantages relative to other methods based on the CWT (Diallo et al. 2005; Diallo et al., 2006; Kulesh et al., 2007). The signal can be very accurately recovered from the time-frequency domain to the time domain, while any real mother wavelet can be used.

With respect to other methods based on time domain only analysis, such as CTA, the proposed method identifies and separates different waves of the signal, even when they occur simultaneously in time, under the condition that they have different polarization characteristics.

The proposed algorithm identifies and extracts automatically the different waves of a signal, depending on the reciprocal ellipticity. Moreover, the algorithm is flexible and provides sufficient information to the user, who may also manually

select the reciprocal ellipticity intervals to extract the corresponding waves in the signals.

The proposed method and the automatic extraction algorithm have been evaluated on synthetic signals. For all the analyzed cases, the algorithm identified and extracted properly all the different waves of the signal, according to the respective reciprocal ellipticity values. Comparing the estimated waves of the signal with the synthetics ones, correlation coefficients above 0.98 were obtained.

The proposed method has also been applied to real signals. In this case, it is not possible to evaluate in an objective way the quality of the obtained results, but based on experience, it is possible to qualitatively evaluate which phases are isolated correctly.

For the analyzed cases, the proposed method provides automatically a set of reciprocal ellipticity intervals that might, with large degree of confidence, be assigned to phases existing in the signal. From the results returned by analyzing both synthetic and real signals, we can conclude that the proposed method identifies and extracts automatically the linearly and elliptically polarized waves of a signal, discerning clearly both types of polarization. This is very important in seismological applications (reflection/refraction experiments and microzonation studies), as it allows, to a first order, the separation of the body waves (linearly polarized) from the Rayleigh waves (elliptically polarized). Moreover, the proposed method can identify and extract also waves with different elliptical polarizations, allowing us to better understand the time-frequency polarization of Rayleigh waves.

For the analyzed cases, the polarization analysis has been carried out using

the vertical and radial components. However, generalizing the use of this method to other orthogonal components should be also possible.

Acknowledgments

This work has been carried out thanks to the financial support of the Spanish Government (MARSH- CGL2007-62454). The Geophysical Instrument Pool Potsdam (GFZ) provided instruments for the experiment in Bonn. We are also very grateful to GFZ German Research Center for Geosciences that provided the means needed for the collaboration. K. Fleming kindly improved our English. Finally, we thank to the editor-in-chief, Dimitri E. Beskos, and the anonymous reviewer for their comments which helped us to clarify and improve this paper. The computer code can be made available directly contacting the authors.

References

Anant, K. and F. Dowla. (1997). Wavelet transform methods for phase identification in three-component seismograms, *Bull. Seismol. Soc. Am.*, 87, 1598-1612.

Daubechies, I. (1992). "Ten lectures on wavelets," in CBMS-NSF Reg. Conf. Series Appl. Math. Philadelphia, PA: SIAM, vol. 61.

D'Auria, L., F. Giudicepietro, M. Martini, M. Orazi, R. Peluso, and G. Scarpato (2010). Polarization analysis in the discrete wavelet domain: An application to volcano seismology, *Bull. Seism. Soc. Am.*, **100–2** , 670-683.

Diallo, M. S., M. Kulesh, M. Holschneider and F. Scherbaum (2005). Instantaneous polarization attributes in the time-frequency domain and wavefield separation. *Geophysical Prospecting*, **53**, 723-731.

Diallo, M. S., M. Kulesh, M. Holschneider, F. Scherbaum and F. Adler (2006). Characterization of polarization attributes of seismic waves using continuous wavelet transform. *Geophysics*, **71**, 67-77.

Donoho, D. and Iain M. Johnstone (1994). Ideal Spatial Adaptation by Wavelet Shrinkage, *Biometrika,* **81,** 425-455.

Farnbach J.S. (1975). The complex envelope in seismic signal analysis, *Bulletin of the Seismological Society of America*, **65**, 951-962.

Gabor, D. (1946). Theory of communication, *Journal IEE* **46**, 429-457.

Galiana-Merino, J.J., J. Rosa-Herranz, J. Giner, S. Molina, and F. Botella (2003). De-Noising of Short Period Seismograms by Wavelet Packet Transform, *Bull. Seism. Soc. Am.*, **93–6** , 2554-2562.

Galiana-Merino, J.J., J. Rosa-Herranz, P. Jauregui, S. Molina and J. Giner (2007). Wavelet transform methods for azimuth estimation on local three-component seismograms, *Bull. Seism. Soc. Am.*, **97–3** , 793-803.

Galiana-Merino, J.J., J. Rosa-Herranz and S. Parolai (2008). Seismic P Phase Picking Using a Kurtosis-Based Criterion in the Stationary Wavelet Domain. IEEE Transactions on Geosciences and Remote Sensing, **46-11**, 3815-3826.

Kulesh, M., M. S. Diallo, M. Holschneider, K. Kurennaya, F. Krüger, M. Ohrnberger and F. Scherbaum (2007). Polarization analysis in the wavelet domain based on the adaptative covariance method. *Geophysical Journal International*, **170**, 667-678.

Kulesh, M., M. Holschneider and M. S. Diallo (2008). Geophysical wavelet library: Applications of the continuous wavelet transform to the polarization and dispersion analysis of signals. *Computers & Geosciences*, **34-12**, 1732-1752.

Li X. L. and S. Crampin (1991). Complex component analysis of shear wave splitting: theory. *Geophysical Journal International*, **107**, 597-604.

Morozov I. B. and S. B. Smithson (1996). Instantaneous polarization attributes and directional filtering. *Geophysics*, **61**, 872-881.

Nason, N. P. and B. W. Silverman (1995) The stationary wavelet transform and some statistical applications, *Lecture Notes in Statistics*, vol. 103, pp. 281-299.

Ohrnberger M., F. Scherbaum, F. Krüger, R. Pelzing, and S.K. Reamer (2003). How good are shear wave velocity models obtained from inversion of ambient vibrations in the Lower Rhine Embayment (N.W. Germany). *Bolletino di Geofisica Teorica e' Applicata*, **45**, 215-232.

Parolai, S., S. M. Richwalski, C. Milkereit, and D. Fäh (2006). S-wave velocity profiles for earthquake engineering purposes for the Cologne area (Germany), Bull. Earth. Eng. 4, 65–94.

René R. M., J. L. Fitter, P. M. Forsyth, K. Y. Kim, D. J. Murray, J. K. Walters and J. D. Westerman (1986). Multicomponent seismic studies using complex trace analysis. *Geophysics*, **51**, 1235-1251.

Richwalski, S., Picozzi, M., Parolai, S., Milkereit, C., Baliva, F., Albarello, D., Roy-Chowdhury, K., Van der Meer, H., Zschau, J., 2007. Raleigh wave dispersion curves from seismological and engineering-geotechnical methods: a comparison at the Bornheim test site (Germany). J Geophysics and Eng. 4, 349-361

Scherbaum, F., K.G. Hinzen, and M. Ohrnberger (2003). Determination of shallow shear wave velocity profiles in the Cologne/Germany area using ambient vibrations. *Geophysical Journal International*, **152**, 597-612.

Shieh, C. F. and R. B. Herrmann (1990). Ground roll: Rejection using polarization filters. *Geophysics*, **55**, 1216-1222.

Steeghs, P. (1997) Local Power Spectra and Seismic Interpretation, Ph.D. Thesis, Delft University of Technology, The Netherlands, 1997.

Taner, M. T. and R. E. Sheriff (1977). Application of amplitude, frequency, and other attributes to stratigraphic and hydrocarbon determination, in Payton, C. E., Ed., Application to hydrocarbon exploration, *Am. Assn. Petr. Geol. Memoir*, **26**, 301-327.

Taner, M. T., F. Koehler and R. E. Sheriff (1979). Complex seismic trace analysis. *Geophysics*, **44**, 1041-1063.

Vidale J.E. (1986). Complex polarization analysis of particle motion, *Bulletin of the Seismological Society of America*, **76**, 1393-1405.

Wickerhauser, M. V. (1994). *Adapted Wavelet Analysis from Theory to Software*, A.K. Peters, Ltd., Wellesley.

Table 1

Correlation coefficients between the different consecutive signals (Figure 7a) obtained from the filtering process

Reciprocal ellipticity intervals	**Correlation coefficient**
[0.0 , 0.1] – [0.0 , 0.2]	1.0000
[0.0 , 0.2] – [0.0 , 0.3]	0.9998
[0.0 , 0.3] – [0.0 , 0.4]	1.0000
[0.0 , 0.4] – [0.0 , 0.5]	0.7009
[0.0 , 0.5] – [0.0 , 0.6]	0.8232
[0.0 , 0.6] – [0.0 , 0.7]	1.0000
[0.0 , 0.7] – [0.0 , 0.8]	1.0000
[0.0 , 0.8] – [0.0 , 0.9]	1.0000
[0.0 , 0.9] – [0.0 , 1.0]	1.0000

Table 2

Correlation coefficients between the estimated waves and the synthetic signal

Wave polarization	**Correlation coefficient (Vertical component)**	**Correlation coefficient (Radial component)**
Linear polarization	0.9987	0.9987
Elliptical polarization 1	0.9894	0.9892
Elliptical polarization 2	0.9876	0.9885

Table 3

Correlation coefficients between the estimated waves and the synthetic signal with noise

Wave polarization	**Correlation coefficient (Vertical component)**	**Correlation coefficient (Radial component)**
Linear polarization	0.9984	0.9984
Elliptical polarization 1	0.9892	0.9889
Elliptical polarization 2	0.9872	0.9881

Figure captions:

Fig. 1. Tree structure of the wavelet packet analysis, where *H* and *G* are low-pass and high-pass filters, respectively, and D is a downsampling operator. $\lambda_{j,r}(n)$ are the different signals associated with every node of the decomposition. In this nomenclature, each node is characterized by a pair of numbers (*j*,*r*), where *j* is the scale index and *r* is the index associated with the frequency or the position within a scale.

Fig. 2. Polarization ellipse showing the geometric parameters: semi-major axis (a), semi-minor axis (b), and tilt angle with respect to the vertical (τ).

Fig. 3. General scheme of the proposed method.

Fig. 4. Example of the vertical component of a real signal (a) and the corresponding DSWPT coefficients (b). The associated reciprocal ellipticity values obtained with the vertical and radial components are also shown (c).

Fig. 5. Scheme of the filter bank of reciprocal ellipticity, with $\Delta\varphi = 0.1$.

Fig. 6. Vertical and radial components of the linearly polarized wave (a), the elliptically polarized waves (b, c) and the synthetic signal formed by the union of the three waves (d). On the right-hand side, the polarization ellipsoids for the vertical and radial components are also presented.

Fig. 7. (a) Signal decomposition at different reciprocal ellipticity intervals, between 0 and the reciprocal ellipticity value (0.1, 0,2, …, 1), and (b) the respective differences

between these intervals. For the clarity of this figure, we show only the results at $\Delta\varphi = 0.1$.

Fig. 8. Correlation coefficients between the different consecutive sub-signals obtained from the filtering process (synthetic signal).

Fig. 9. Comparison between the estimated waves of the signal (black color) and the initial synthetic waves (gray color). (a) Linearly polarized wave, (b) elliptically polarized wave 1, and (c) elliptically polarized wave 2. On the right-hand side, the polarization ellipsoids for the vertical and radial components are also presented.

Fig. 10. Correlation coefficients between the different consecutive sub-signals obtained from the filtering process (synthetic signal contaminated with noise).

Fig. 11. Comparison between the estimated waves of the signal (black color) and the initial synthetic waves (gray color). (a) Linearly polarized wave, (b) elliptically polarized wave 1, and (c) elliptically polarized wave 2. On the right-hand side, the polarization ellipsoids for the vertical and radial components are also represented.

Fig. 12. Deployment of the source and the linear array of geophones for the experiment carried out in Bonn (Germany).

Fig. 13. Real three-component signal recorded by geophone 9 for the experiment carried out in Bonn (Germany).

Fig. 14. Correlation coefficients between the different consecutive sub-signals obtained from the filtering process (real signal).

Fig. 15. Vertical and radial components of the recorded signal and the estimated waves obtained from the different estimated reciprocal ellipticity intervals. On the right-hand side, the polarization ellipsoids for the vertical and radial components are also represented.

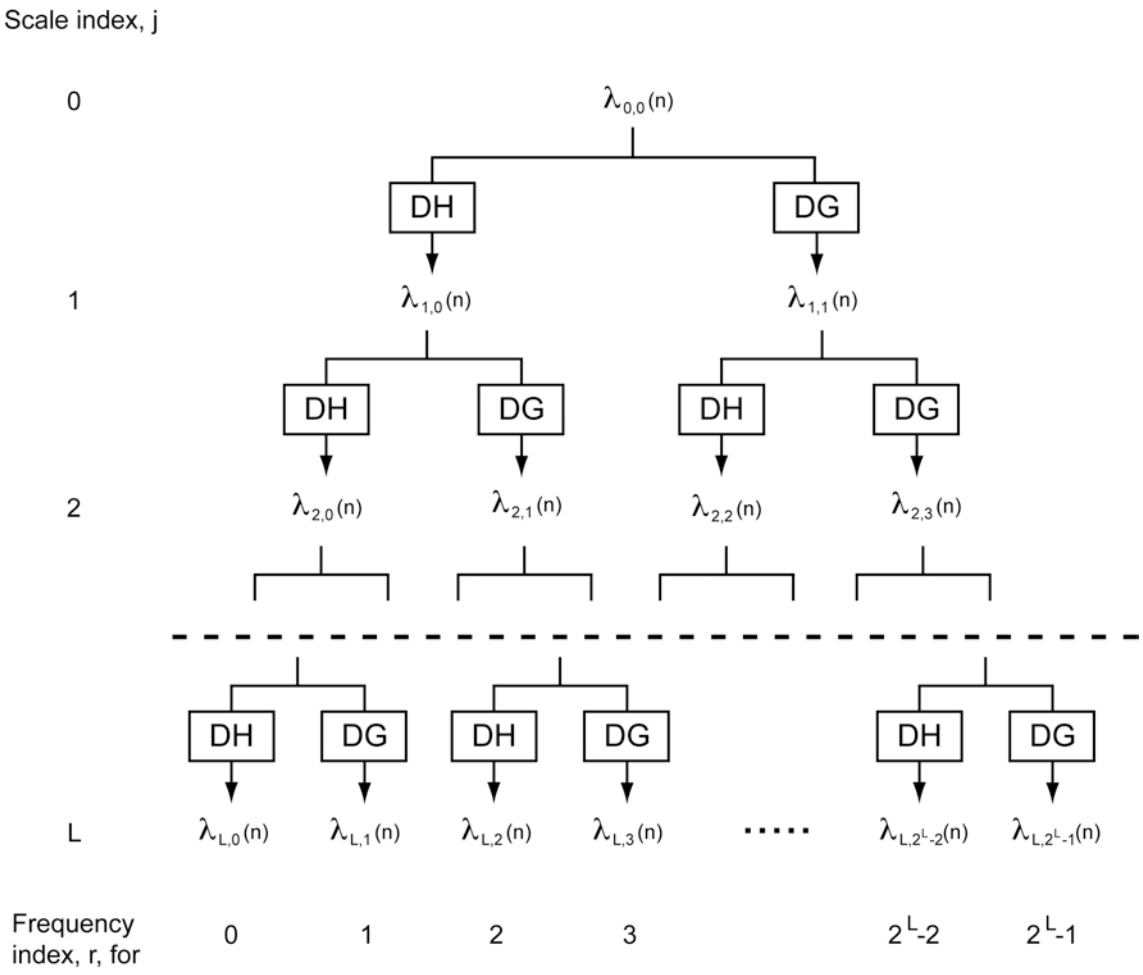

Fig. 1. Tree structure of the wavelet packet analysis, where *H* and *G* are low-pass and high-pass filters, respectively, and D is a downsampling operator. $\lambda_{j,r}(n)$ are the different signals associated with every node of the decomposition. In this nomenclature, each node is characterized by a pair of numbers (*j*,*r*), where *j* is the *scale* index and *r* is the index associated with the frequency or the position within a scale.

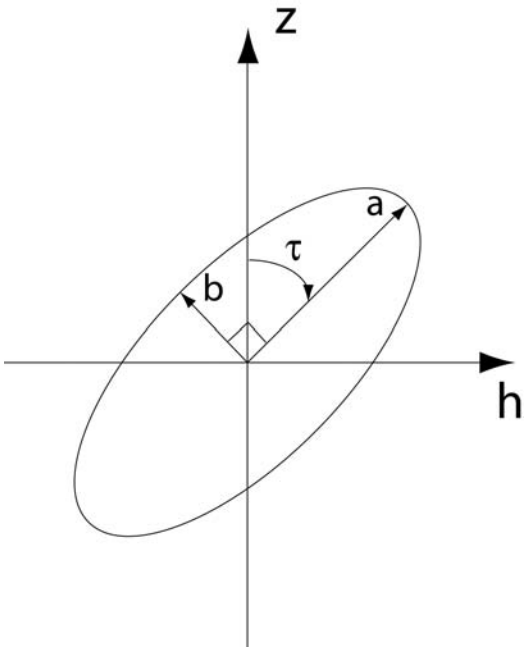

Fig. 2. Polarization ellipse showing the geometric parameters: semi-major axis (a), semi-minor axis (b), and tilt angle with respect to the vertical (τ).

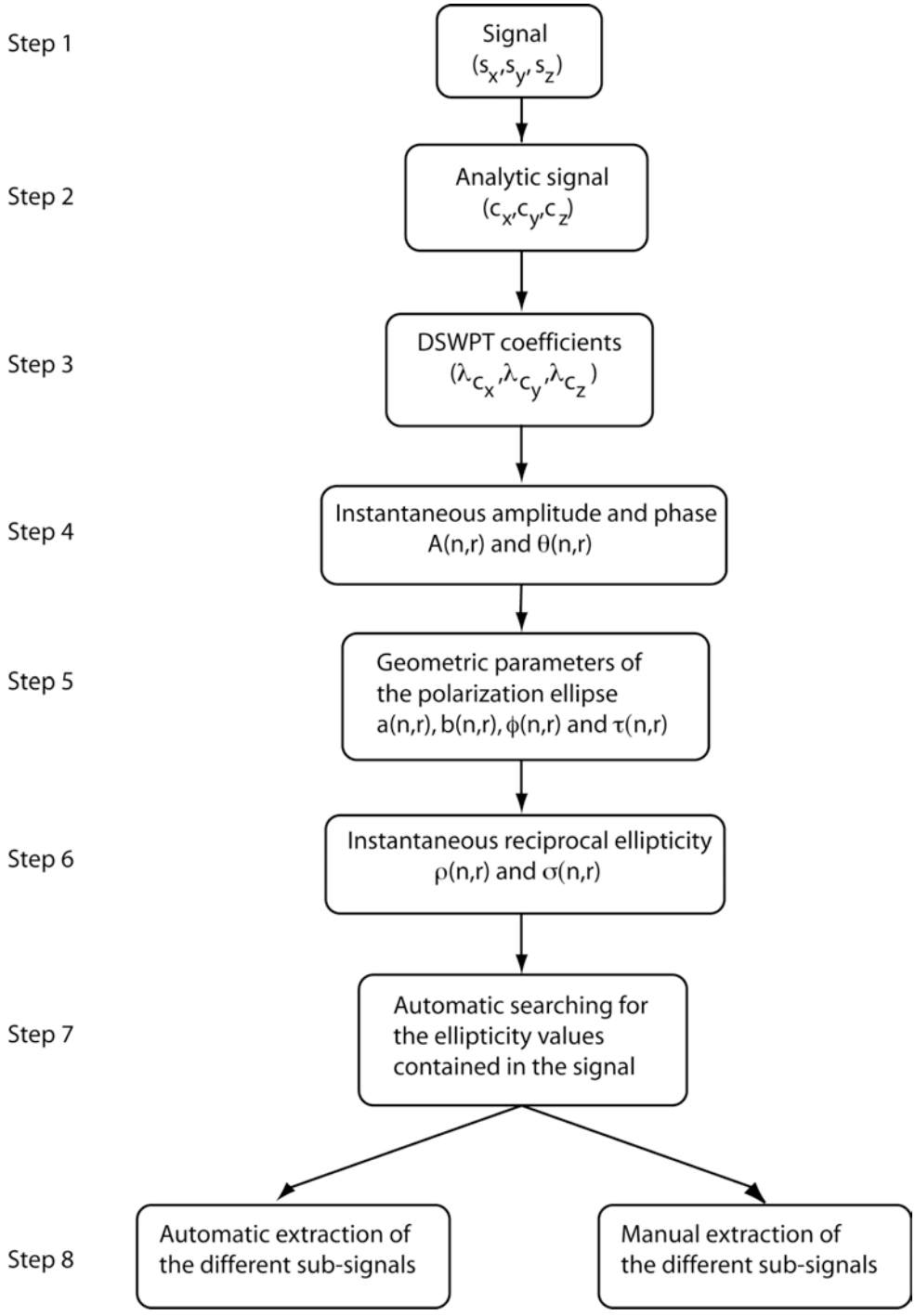

Fig. 3. General scheme of the proposed method.

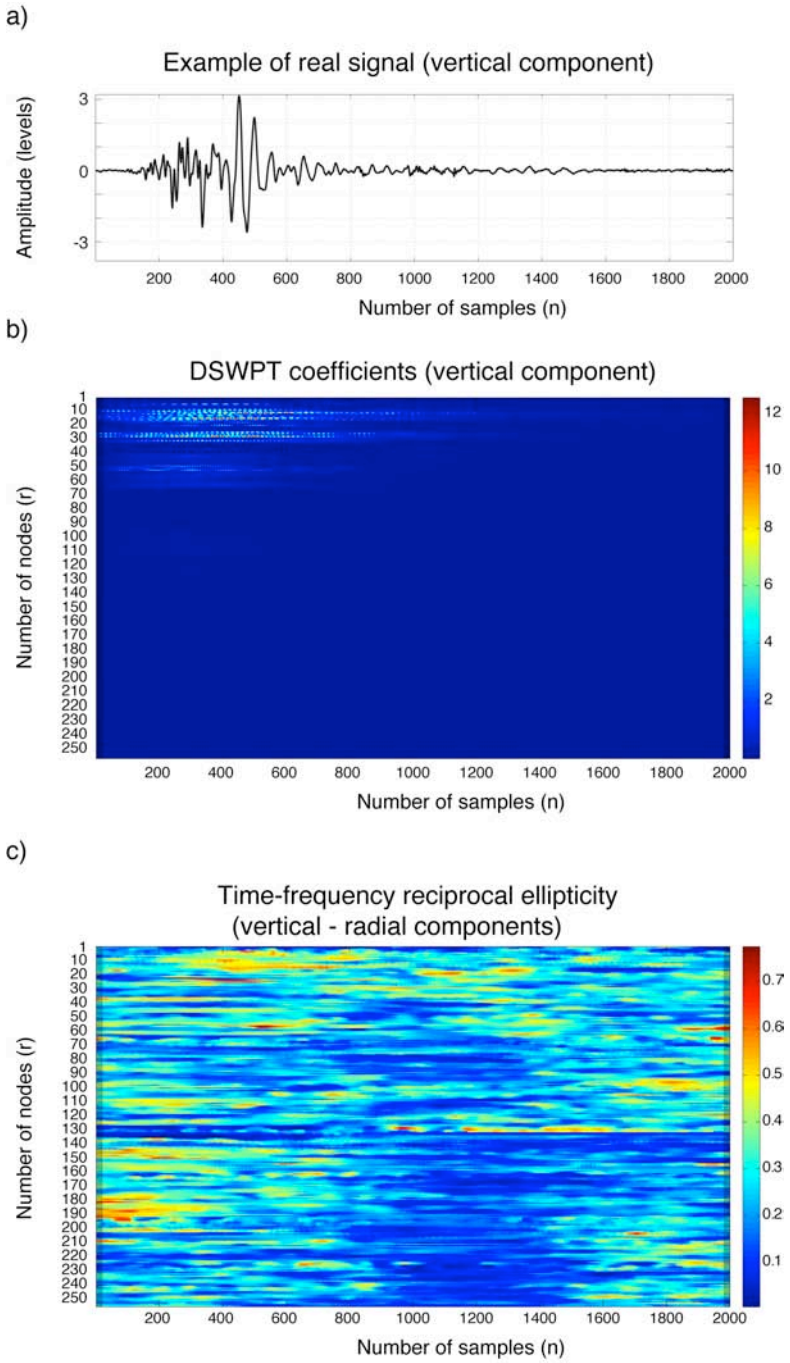

Fig. 4. Example of the vertical component of a real signal (a) and the corresponding DSWPT coefficients (b). The associated reciprocal ellipticity values obtained with the vertical and radial components are also shown (c).

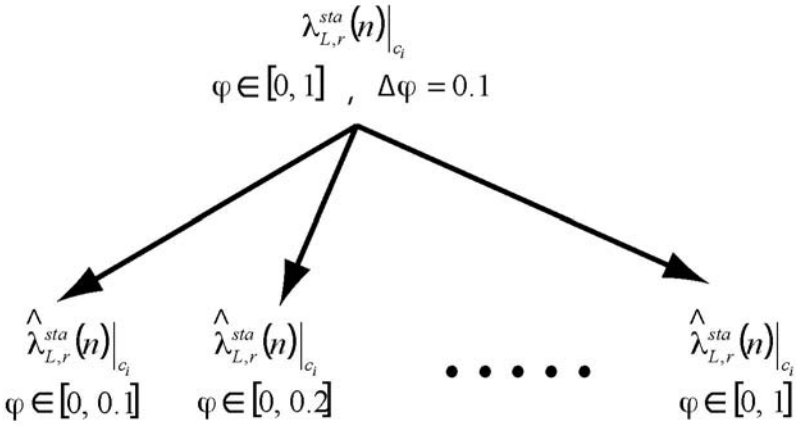

Fig. 5. Scheme of the filter bank of reciprocal ellipticity, with $\Delta\varphi = 0.1$.

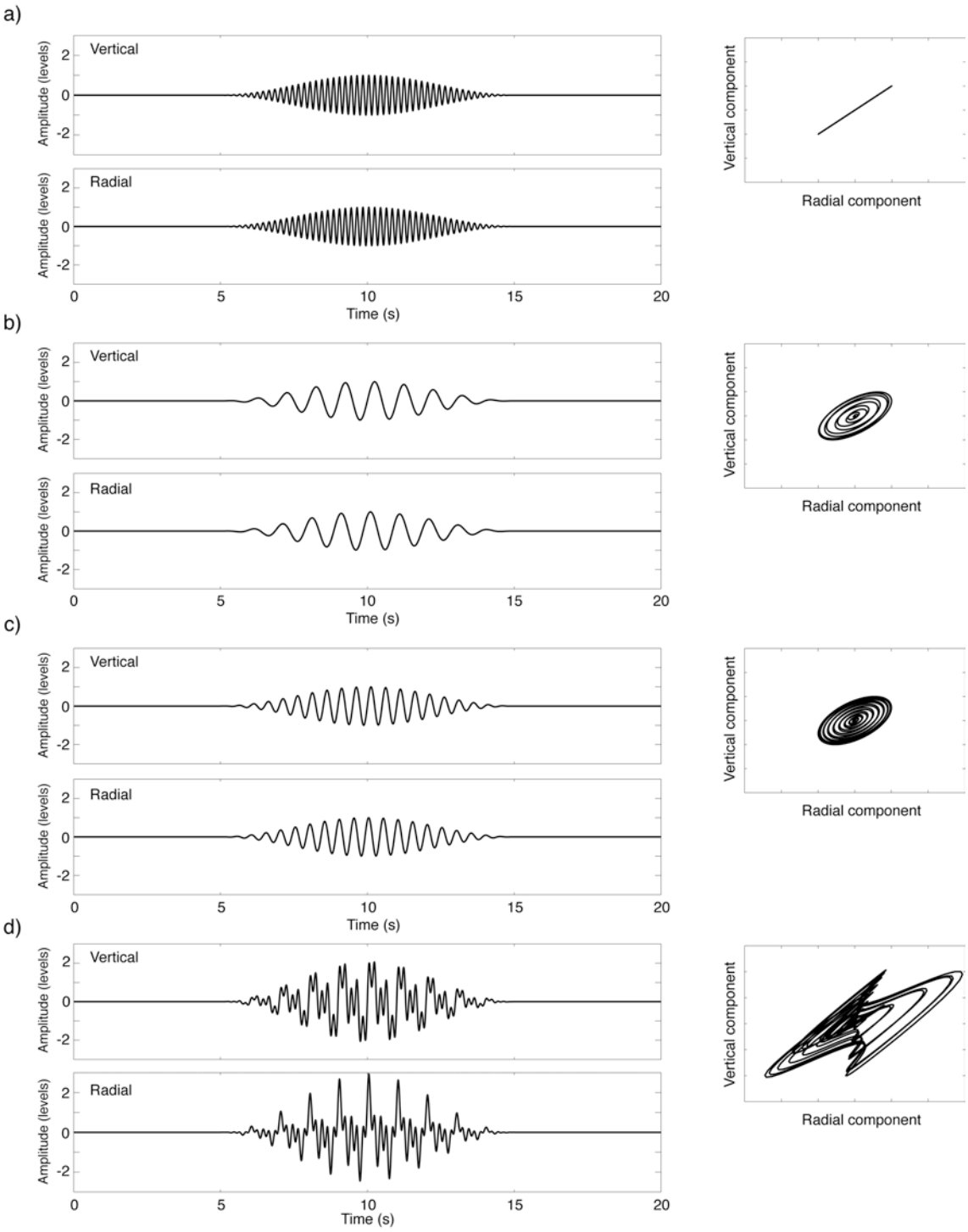

Fig. 6. Vertical and radial components of the linearly polarized wave (a), the elliptically polarized waves (b, c) and the synthetic signal formed by the union of the three waves (d). On the right-hand side, the polarization ellipsoids for the vertical and radial components are also presented.

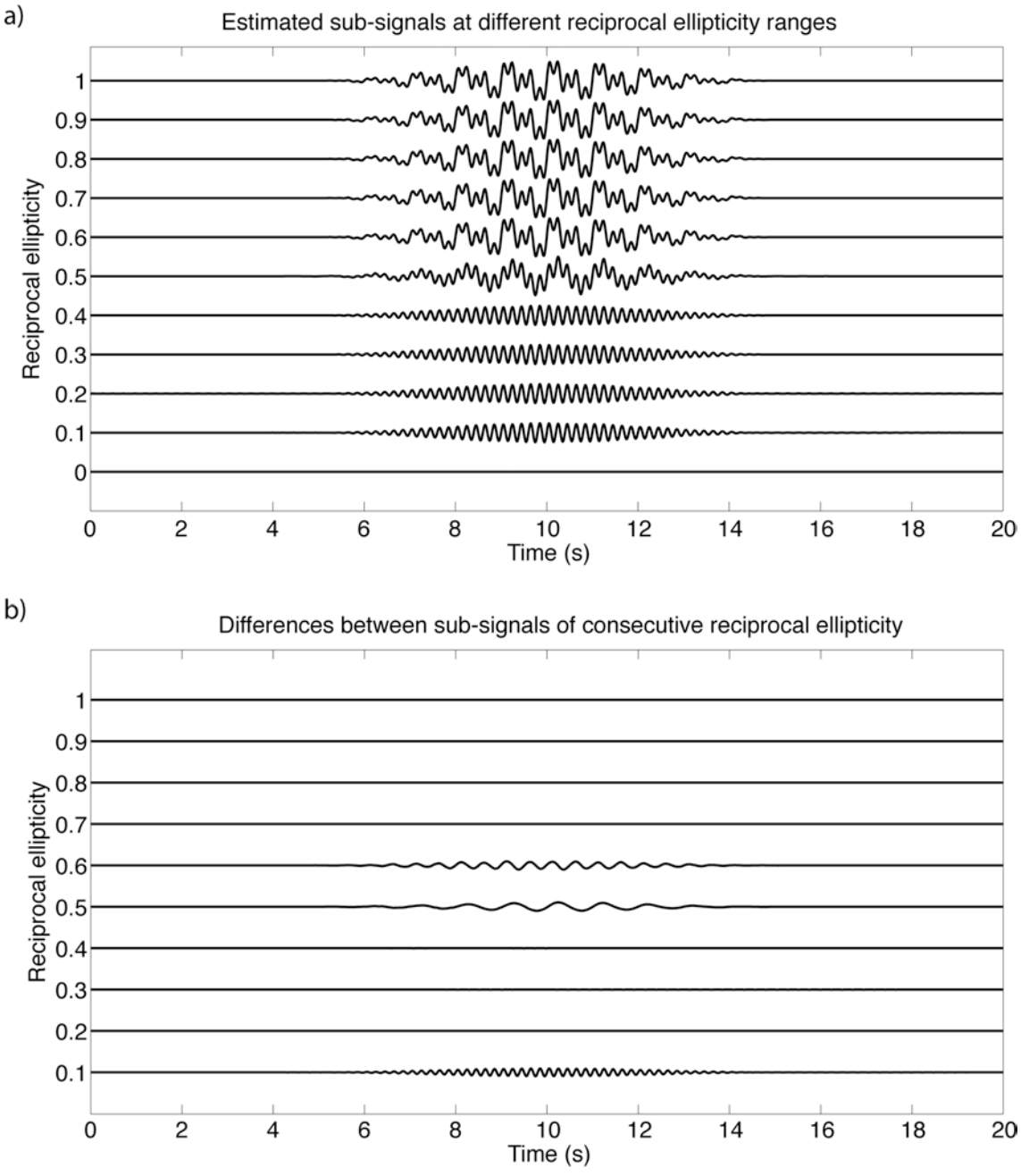

Fig. 7. (a) Signal decomposition at different reciprocal ellipticity intervals, between 0 and the reciprocal ellipticity value (0.1, 0,2, …, 1), and (b) the respective differences between these intervals. For the clarity of this figure, we show only the results at $\Delta\varphi = 0.1$.

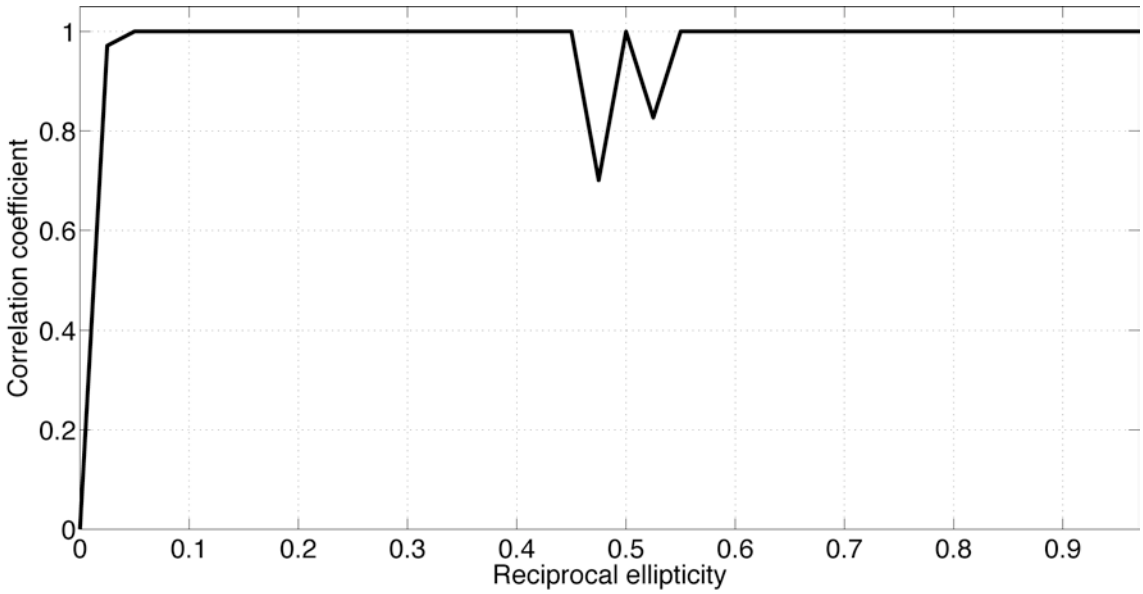

Fig. 8. Correlation coefficients between the different consecutive sub-signals obtained from the filtering process (synthetic signal).

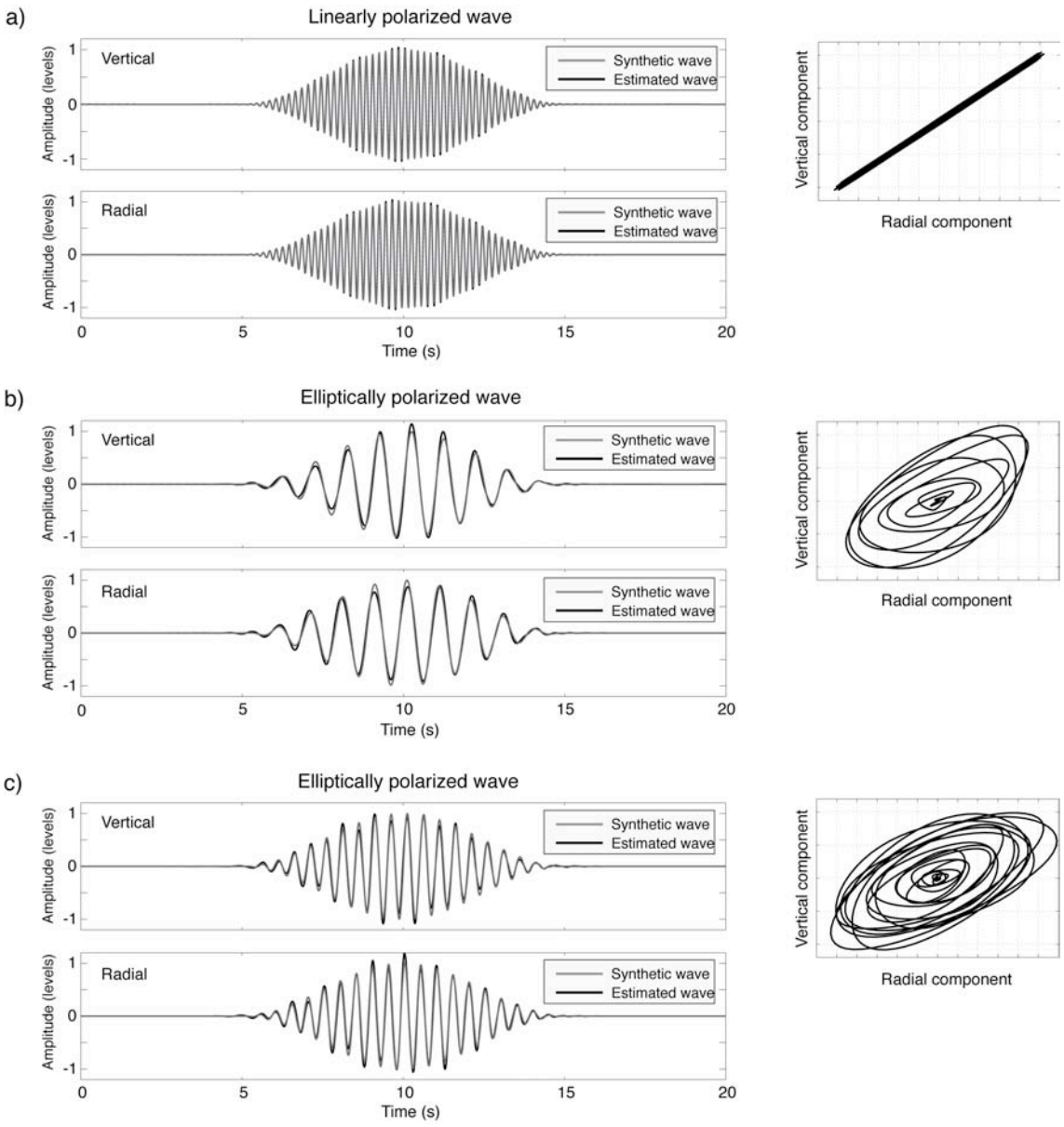

Fig. 9. Comparison between the estimated waves of the signal (black color) and the initial synthetic waves (gray color). (a) Linearly polarized wave, (b) elliptically polarized wave 1, and (c) elliptically polarized wave 2. On the right-hand side, the polarization ellipsoids for the vertical and radial components are also presented.

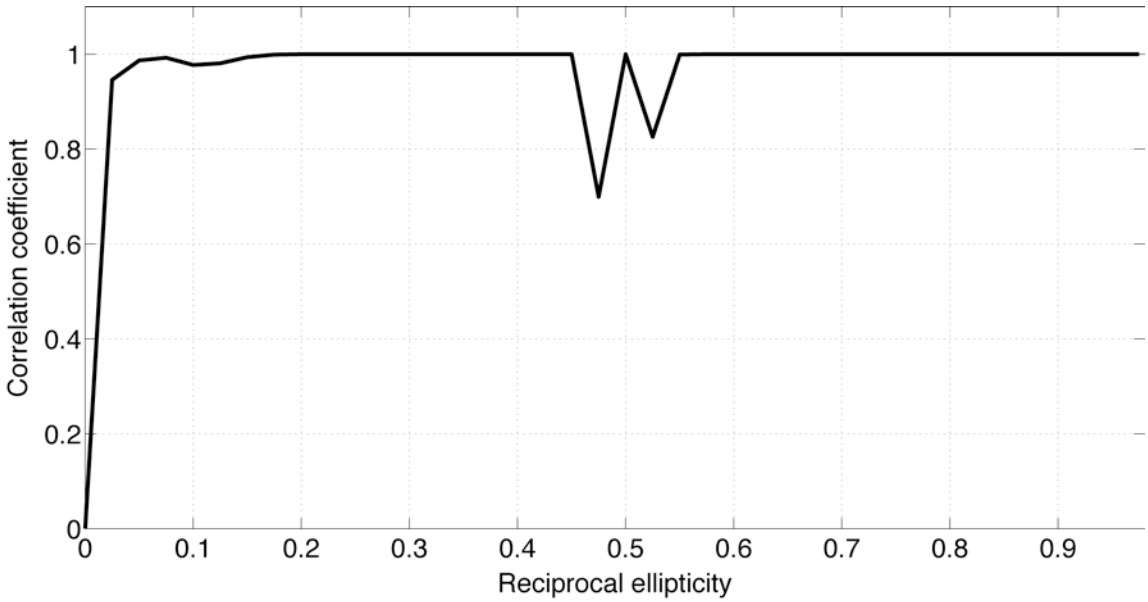

Fig. 10. Correlation coefficients between the different consecutive sub-signals obtained from the filtering process (synthetic signal contaminated with noise).

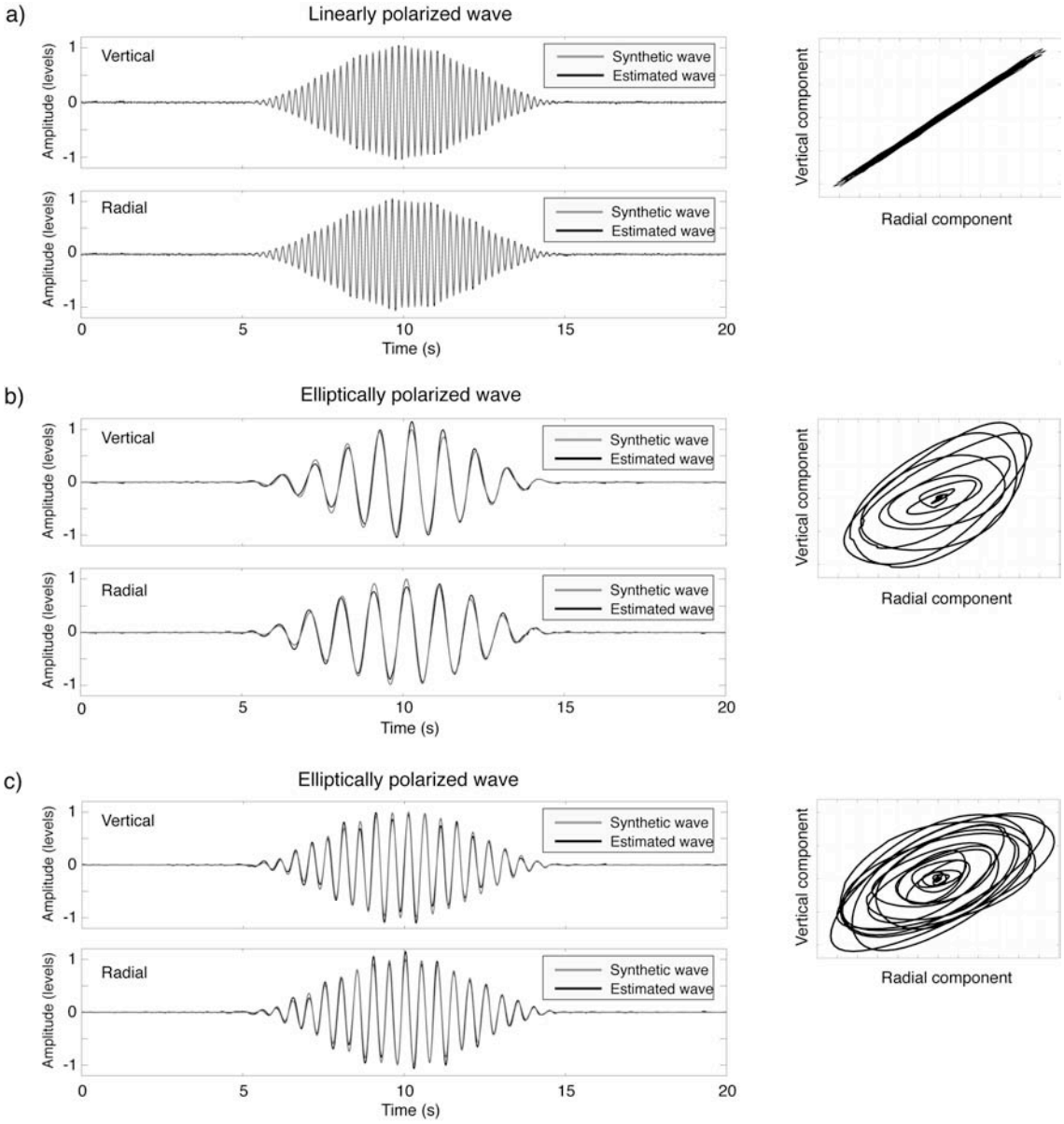

Fig. 11. Comparison between the estimated waves of the signal (black color) and the initial synthetic waves (gray color). (a) Linearly polarized wave, (b) elliptically polarized wave 1, and (c) elliptically polarized wave 2. On the right-hand side, the polarization ellipsoids for the vertical and radial components are also represented.

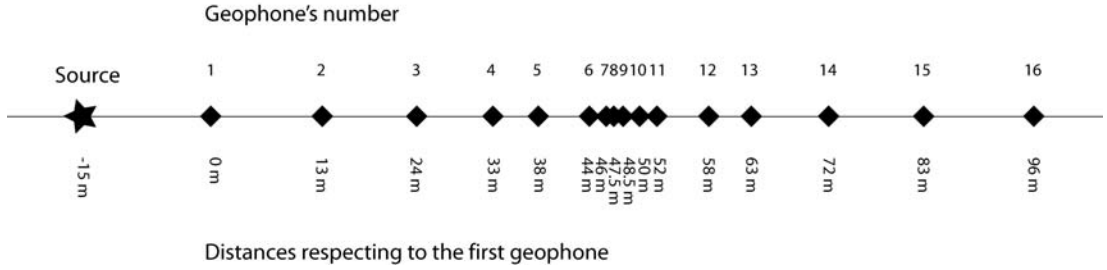

Fig. 12. Deployment of the source and the linear array of geophones for the experiment carried out in Bonn (Germany).

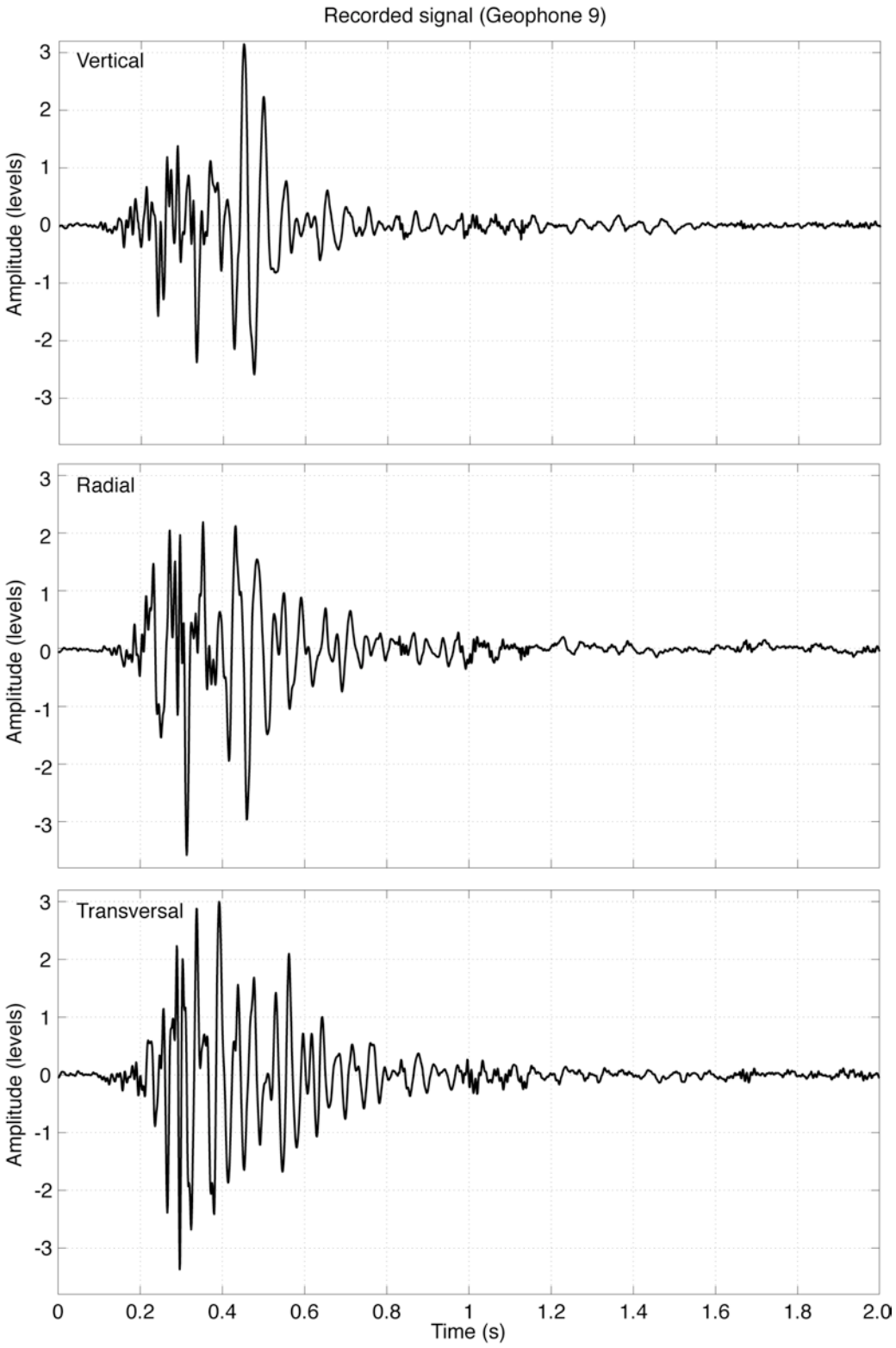

Fig. 13. Real three-component signal recorded by geophone 9 for the experiment carried out in Bonn (Germany).

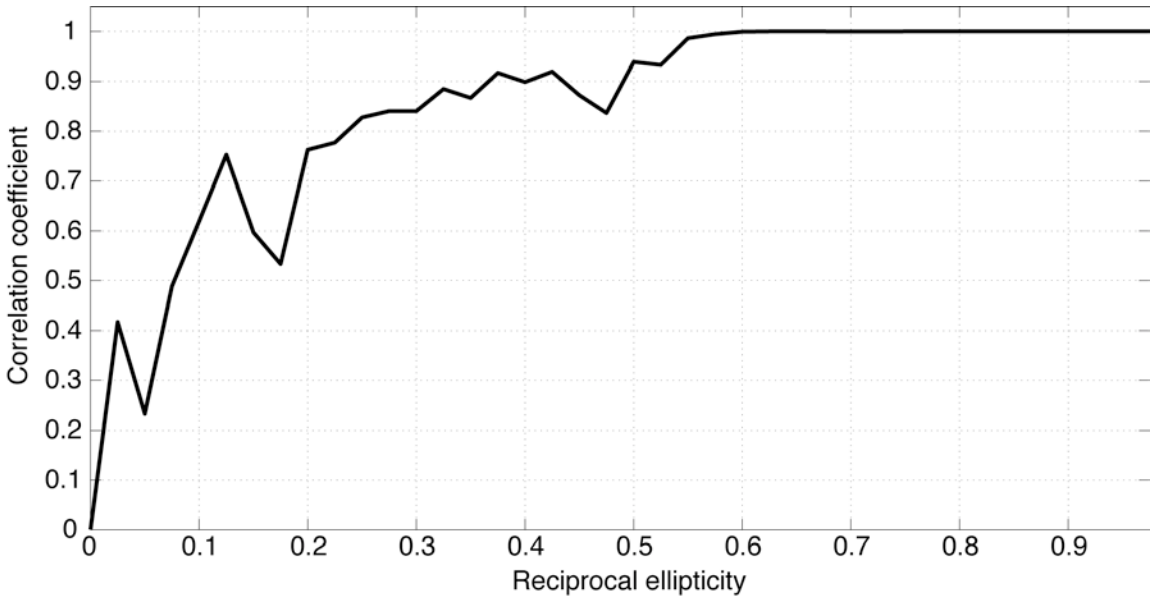

Fig. 14. Correlation coefficients between the different consecutive sub-signals obtained from the filtering process (real signal).

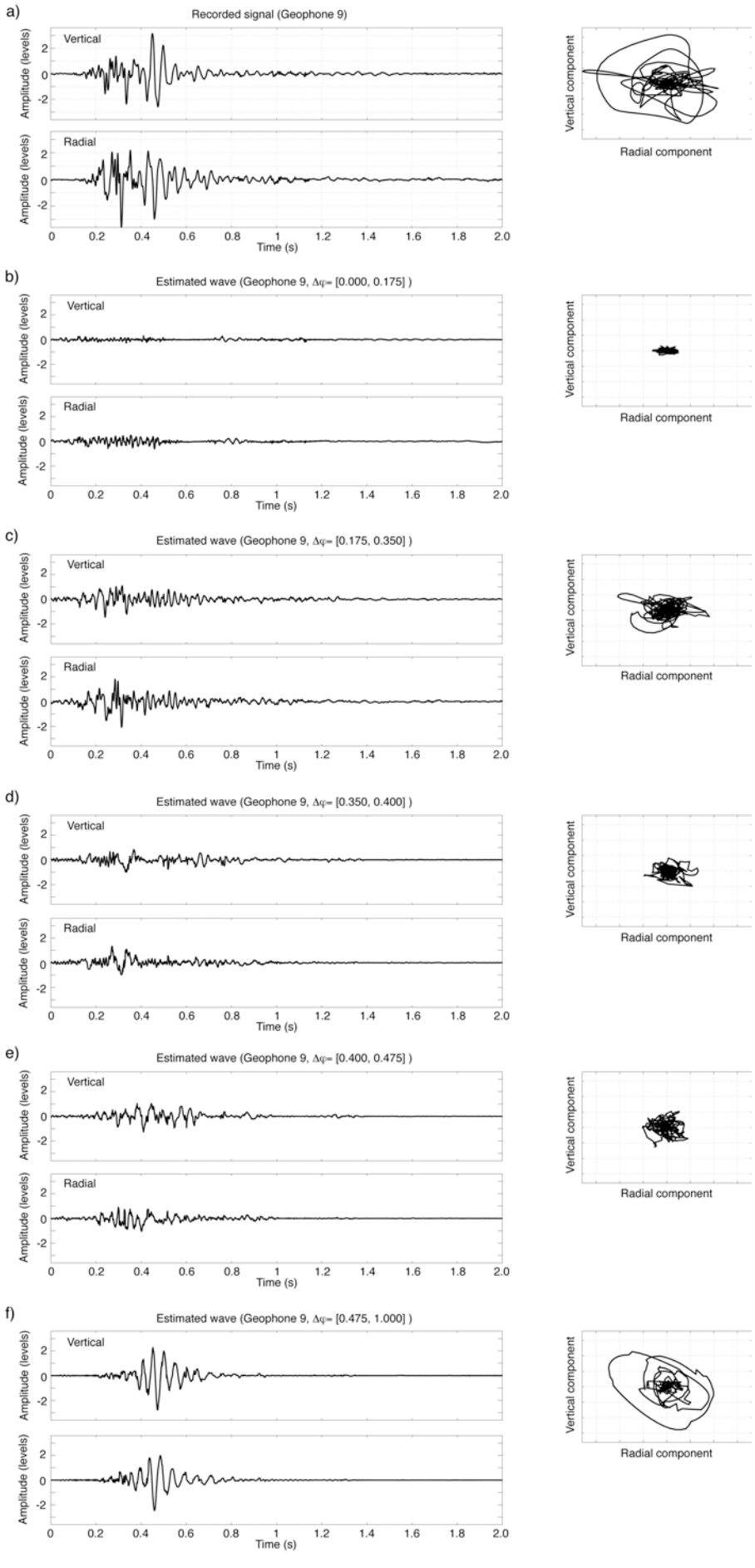
a)
Recorded signal (Geophone 9)
Vertical
Radial
Amplitude (levels)
Time (s)
Vertical component
Radial component
b)
Estimated wave (Geophone 9, Δφ= [0.000, 0.175])
c)
Estimated wave (Geophone 9, Δφ= [0.175, 0.350])
d)
Estimated wave (Geophone 9, Δφ= [0.350, 0.400])
e)
Estimated wave (Geophone 9, Δφ= [0.400, 0.475])
f)
Estimated wave (Geophone 9, Δφ= [0.475, 1.000])

Fig. 15. Vertical and radial components of the recorded signal and the estimated waves obtained from the different estimated reciprocal ellipticity intervals. On the right-hand side, the polarization ellipsoids for the vertical and radial components are also represented.